BPT-4000 Hall Thruster Discharge Chamber Erosion Model Comparison with Qualification Life Test Data

IEPC-2007-267

Presented at the 30th International Electric Propulsion Conference, Florence, Italy
September 17-20, 2007

Richard R. Hofer,[*] Ioannis G. Mikellides,[†] Ira Katz,[‡] and Dan M. Goebel[§]
Jet Propulsion Laboratory, California Institute of Technology, Pasadena, CA 91109

Commercial electric propulsion systems are now being considered as a cost effective solution for competitively awarded science missions such as the NASA Discovery and New Frontiers programs. Aerojet's BPT-4000 Hall thruster, which has been identified as a candidate for near-term use on NASA science missions, has recently completed a 6,750 h qualification life test that demonstrated power throttling from 1 to 4.5 kW and a total impulse of 5.3 MN-s. The implementation of electric propulsion technology on NASA science missions requires the availability of life models that can accurately reproduce the erosion observed during ground testing as well as predict the erosion for actual mission profiles. Hall thruster simulations are presented from an erosion model developed at JPL in concert with a modified version of the plasma model HPHall-2. The models are applied to the BPT-4000 and used to calculate the performance and erosion observed during qualification life testing. The models are shown to be capable of accurately reproducing many of the micro- and macroscopic properties that determine the plasma response and thruster performance over a wide range of power and voltages. An erosion simulation carried through almost 1000 hours of thruster operation has shown general agreement overall with experiment. Analysis of wall erosion properties reveals that the process is both spatially and temporally dependent, which verifies the importance of developing modeling tools that are physics-based and capable of predicting the complexity of Hall thruster erosion physics.

---

[*] Member of the Technical Staff, Electric Propulsion Group, Propulsion and Materials Engineering Section, 4800 Oak Grove Drive, Mail Stop 125-109; richard.r.hofer@jpl.nasa.gov. Senior Member AIAA.

[†] Member of the Technical Staff, Electric Propulsion Group, Propulsion and Materials Engineering Section. Senior Member AIAA.

[‡] Group Supervisor, Electric Propulsion Group, Propulsion and Materials Engineering Section. Senior Member AIAA.

[§] Senior Research Scientist, Propulsion and Materials Engineering Section. Senior Member AIAA.

I. Introduction

COMMERCIAL electric propulsion systems are now being considered as a cost effective solution for competitively awarded science missions such as the NASA Discovery and New Frontiers programs [1-4]. Many of the missions being studied would require wider power throttling capabilities and longer thruster life compared to commercial applications. These differences can be addressed through a combination of delta-qualification testing and modeling [1,4]. In this paper, we discuss continuing efforts at the Jet Propulsion Laboratory (JPL) to develop predictive models of Hall thruster performance and erosion. The aim of this work is to provide NASA with a set of physics-based modeling tools that can be used to address the qualification gaps between ground testing and actual mission requirements.

The service life of electric propulsion systems has been customarily demonstrated through multi-year life ground tests that typically cost several million dollars. For example, the Extended Life Test (ELT) of the 2.3 kW NSTAR ion thruster was completed in 2004 after more than 30,000 h of operation at JPL and was the longest life test of an ion thruster ever conducted [5]. In 2005, the qualification life test (QLT) for geosynchronous earth orbit (GEO) applications of Aerojet's BPT-4000 Hall thruster was completed [6,7]. The potential mission benefits of the BPT-4000 prompted NASA to fund a low-power qualification life test extension (QLT-E) at 1-2 kW that brought the total operating time to 6,750 h for a qualified power throttling range of 1 to 4.5 kW [8]. As NASA missions become more demanding both the cost and time associated with life tests is expected to rise. While some flagship missions may be able to absorb such costs, launch window opportunities and mission timelines may simply rule out long-duration life testing regardless of the mission class.

Regardless of the technology under consideration, the implementation of an electric propulsion system on a NASA science mission requires the availability of life models that can accurately calculate the erosion observed during ground testing as well as predict the erosion for actual mission profiles. This need is driven simply by the fact that the qualification life test is unlikely to exactly match the mission profile for the first use of the technology, let alone the n^{th} use.

Influenced by all of these factors, a rigorous life-modeling program has been ongoing at JPL for the past several years in an effort to establish a thruster life qualification capability aimed at decreasing or eliminating the cost and time required to assess thruster service life through time-consuming and expensive life testing [9-12]. A major focus is currently the development of plasma and erosion models of Hall thruster discharge chambers.

Hall thruster life is primarily limited by erosion of the discharge chamber walls due to high-energy ion sputtering that eventually exposes the magnetic circuit. Hall thrusters continue operating long after the magnetic circuit is first exposed [13,14], often without significant performance changes, and for this reason this moment in time is sometimes called a "soft failure." Whether or not a spacecraft can tolerate deposition from the metallic sputter products of the now exposed magnetic circuit is mission dependent. Given a sufficiently long enough time the gradual erosion of the magnetic circuit would presumably lead first to performance degradation and eventually to difficulties starting and maintaining the plasma

discharge. However, to our knowledge this hard failure point has never been documented in a long duration life test, but is known to be at least several thousand hours of additional operation [13,14].

To better understand these mechanisms the computational effort at JPL has made use of existing models wherever applicable [15,16], and has developed new models or extensions to existing models as deemed necessary [9-11,17]. Our approach has intentionally avoided semi-empirical or low-order fluid models that fail to capture enough of the relevant physics to be solely relied on as a predictive tool for missions costing hundreds of millions of dollars [18-21]. This is motivated by our need to understand Hall thruster physics and failure modes over the power throttling range required by deep-space missions without complete reliance on empirical data or simulations that can not adequately model the relevant plasma instabilities (and any possible anomalous erosion resulting from them) that are inherent to Hall thruster operation. Accordingly, for our models to be relied on as accurate representations of thruster physics, it is necessary, at a minimum, that they reproduce accurately the time-averaged distribution and magnitudes of plasma properties in the channel as well as the performance and erosion observed over the throttling range.

We are continuing to improve our Hall thruster discharge chamber plasma and erosion models and have applied these models to the SPT-100, BPT-4000, and several NASA thrusters. This is a continuation of previous works reported in Ref. [9-11] that utilized a modified version of HPHall-2 [15,16]. HPHall is an axisymmetric solver that employs a hybrid fluid/particle-in-cell (hybrid-PIC) numerical approach to simulate the evolution of the plasma inside the discharge chamber and near-field plume of a Hall thruster. HPHall, originally developed by Fife and Martínez-Sánchez [15], was upgraded by Parra and Ahedo [16], resulting in the latest release, HPHall-2. Throughout this paper, we present results using HPHall-2 with additional JPL modifications. Other researchers are also pursuing hybrid-PIC based models for erosion calculations [22,23]. Sommier, et al [22] have applied their model to the Stanford Hall thruster and SPT-100 while Cheng [23] has used a version of HPHall-2 to model the Busek BHT-200 and BHT-600 thrusters.

In this paper, we present our latest modifications to our plasma and erosion models and apply those models to calculate the plasma response and discharge chamber erosion of the BPT-4000. Modifications include activating the doubly-charged ion model in HPHall-2, updates to several collision cross-sections, secondary electron emission yields, and sputtering yields, modifications to the enforcement of the Bohm condition at the sheath edge, and modifications to the electron mobility model. The updated models are applied to the BPT-4000 Hall thruster and used to calculate the performance and erosion observed during qualification life testing. The models are shown to be capable of accurately reproducing the spatially- and temporally-dependent processes inherent to Hall thruster erosion physics.

II. Review of BPT-4000 Qualification Life Testing

Shown in Figure 1, Aerojet's BPT-4000 Hall thruster has been identified as a candidate for near-term use on NASA science missions [1]. The BPT-4000 Hall thruster propulsion system (HTPS) was developed through a joint effort between Lockheed Martin Space Systems and Aerojet as a 4.5 kW electric

propulsion system for GEO satellite applications. The qualification life test (QLT) for GEO applications of this system was completed in 2005 [6,7], during which the BPT-4000 demonstrated operation over input powers of 3.0 to 4.5 kW and input voltages of 300 to 400 V for firing durations of 5 minutes to over 200 hours. The first flight of the BPT-4000 is scheduled for 2008.

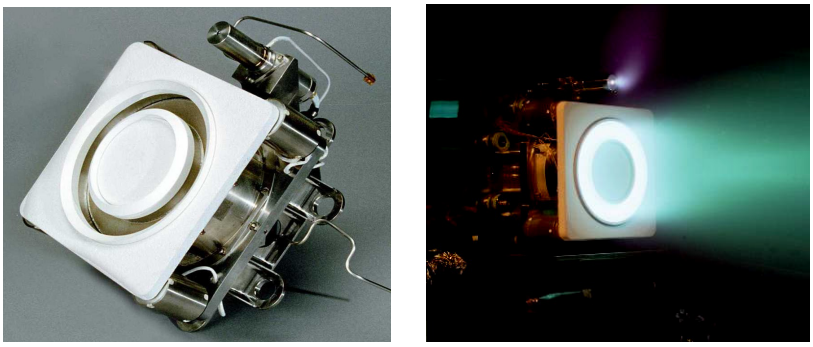

Figure 1. Aerojet BPT-4000 Hall thruster.

A detailed review of the qualification status of a Hall thruster system based on the BPT-4000 for NASA science missions showed no substantial risk items [1]. In most cases, the completed qualification programs for the commercial system equals or exceeds science mission requirements. For those requirements not currently met by commercial components, a low risk delta-qualification has been planned and the cost and risks are manageable.

In order to realize the cost benefits and mission performance of the BPT-4000, it was necessary to demonstrate extended low-power operation of the thruster during a delta-qualification life test. Following the completion of the QLT for GEO applications in late 2005, NASA extended the life test with additional funding in a qualification life test extension (QLT-E).

Table 1 shows the low-power performance of the BPT-4000 during the QLT-E. Figure 2 shows the time history of the BPT-4000 thrust during the QLT-E [24]. During the QLT-E, 950 h of testing (t=5,800-6,750 h) was completed at discharge powers of 1-2 kW [8,24]. To our knowledge, this was the first long-duration life test ever conducted of a Hall thruster at power densities substantially below nominal (in this case, 22% of nominal). Thruster operation was stable and reliable throughout the QLT-E and performance significantly exceeded expectations over the tested range of discharge power. Welander, et al. [8] noted that the efficiency of the 4.5 kW optimized BPT-4000 operating at 1.25-1.5 kW was greater than the SPT-100 and PPS-1350-G thrusters operating at their nominal power of 1.35-1.5 kW.

The QLT-E increased the qualified power throttling range of the BPT-4000 from 3-4.5 kW to 1-4.5 kW. As shown in Table 2, the QLT-E also extended the total operating time and cycles to 6,750 h and 6,844, respectively, while bringing the total xenon processed to 272 kg and the total impulse delivered to 5.3 MN-s [24]. During the QLT-E, the thruster was operated for more than 100 h at each throttle table point from 1 to 2 kW (see Table 3). At 1.5 kW, greater than 480 h was demonstrated. Erosion measurements indicated that very little erosion was observed during the QLT-E. It is estimated by

Aerojet that a total of 12 MN-s and 580 kg of xenon throughput are possible before the magnetic circuit is exposed to the high-energy plasma [4]. The qualified life and throttling capabilities of the BPT-4000 and its low-cost relative to government systems make it a very attractive candidate for near-term infusion in cost-capped science missions such as the NASA Discovery and New Frontiers programs.

Table 1. Low-power performance of the BPT-4000 during the QLT-E (t=5800-6750 h) [24].

Discharge Power, kW	Discharge Voltage, V	Thrust, mN	Total Specific Impulse, s	Total Efficiency*
2.5	400	141	1961	0.54
2.0	400	113	1858	0.51
1.75	350	107	1731	0.52
1.5	300	104	1620	0.55
1.25	250	93	1445	0.53
1.0	200	80	1215	0.48

*Excludes thermally-dependent magnet and cabling losses. At maximum operating temperatures, these losses are typically 1.5% of the total power [6].

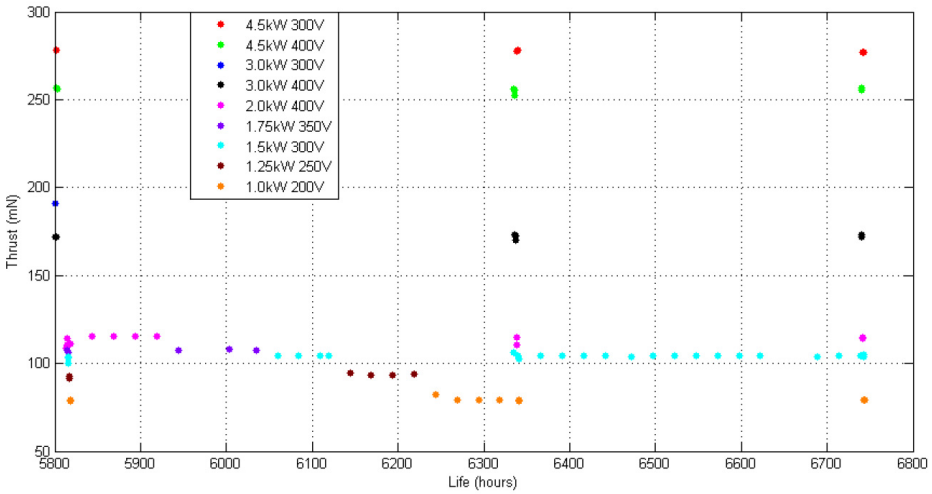

Figure 2. BPT-4000 thrust versus operating time during the QLT-E [24].

Table 2. Demonstrated capability of the BPT-4000 Hall thruster through the end of the Qualification Life Test Extension (QLT-E).

Parameter	BPT-4000 Demonstrated
Total Impulse	5.3 MN-s
Total Firing Time	6,750 h
Total Thruster Starts	6,844
Total Xenon Throughput	272 kg

Table 3. BPT-4000 throttling table through the QLT-E.

Discharge Power, kW	Discharge Voltage, V	Operating Time (h)
4.5	300	2,452
4.5	400	1,250
3.0	300	120
3.0	400	1,797
2.0	400	>100
1.75	350	>100
1.5	300	>480
1.25	250	>100
1.0	200	>100
Total		6,750

III. Model Inputs

All results in this paper are based on information provided by Aerojet of the BPT-4000 design such as geometry, magnetic field, cathode location, wall materials, etc. Most of this information is restricted for public release due to considerations of Aerojet proprietary information and/or export control regulations.

Table 4 presents some of the basic inputs used for the simulations. Table 5 presents the measured beginning-of-life (BOL) performance of the BPT-4000 [25]. Erosion simulations presented here are for the 4.5 kW, 300 V operating condition. The 55x30 grid is structured similar to the one used in simulations of the SPT-100 in Ref. [11]. The BOL anode mass flow rate was computed from the data in Table 5 for an average cathode flow fraction of 7% [6].

Table 4. HPHall inputs for plasma simulations.

Parameter	**Value**
Discharge voltage (V)	300
BOL anode mass flow rate (mg/s)	15.5
Simulation time step (s)	2.5e-8
Grid dimensions	55x30

Table 5. Measured BOL performance of the BPT-4000 [25].

Discharge Power, kW	Discharge Voltage, V	Thrust, mN	Total Specific Impulse, s	Total Efficiency*	Anode Specific Impulse, s**	Anode Efficiency**
4.5	300	291	1788	57	1913	61
4.5	400	253	2020	56	2161	60
3.0	300	199	1719	56	1839	60
3.0	400	174	1967	56	2105	60

*Excludes thermally-dependent magnet and cabling losses. At maximum operating temperatures, these losses are typically 1.5% of the total power [6].

** Computed from total values for an average 7% cathode flow fraction [6].

IV. Model Updates

In this section, we describe updates made to the plasma and erosion models since Ref. [11].

A. Secondary Electron Emission Yield

The yield of secondary electrons from the discharge chamber walls under electron bombardment is an important parameter in the wall sheath model that can significantly affect the plasma response. Ref. [26-33] describe various experimental and theoretical studies for different grades of boron nitride. The uncertainty in the data is typically 10-20% while the number of data points tends to be small, which can lead to variations in the plasma response depending on our choice of parameters. The choice of fit function for the experimental data also influences the plasma response. HPHall has previously fit a power law to experimental data given by

$$\delta_w(E) = \left(\frac{E}{E_1}\right)^{\alpha}, \tag{1}$$

where E is the energy of a monoenergetic beam of electrons taken from experiment, E_1 is the energy where the yield first exceeds unity, and α is a fitting coefficient. This fit function assumes that the yield of electrons goes to zero with the electron energy, which would neglect the effects of backscattering at low energy. Backscattering at low energy can be accounted for by assuming a linear dependence of the yield with energy given by

$$\delta_w(E) = \delta_o + (1-\delta_o)\frac{E}{E_1}, \tag{2}$$

where δ_o is the yield at zero electron energy.

To write the preceding equations in terms of the electron temperature, we average over a Maxwellian distribution and obtain for the power fit

$$\delta_w(T_e) = \Gamma[2+\alpha]\left(\frac{T_e}{E_1}\right)^{\alpha}, \tag{3}$$

where Γ is the gamma function and T_e is the electron temperature. Similarly, the linear fit yields

$$\delta_w\left(T_e\right) = \delta_o + (1-\delta_o)\frac{2T_e}{E_1}. \tag{4}$$

In the present simulations of the BPT-4000, we have updated HPHall-2 to use the linear relationship given by Eqn. (4). The curve fit coefficients are chosen from the literature for the wall material of the BPT-4000.

B. Sputtering Yield

A review of the sputtering yield data for the various grades of boron nitride under xenon bombardment was conducted. Differences in the data are substantial, there is no data at energies below 80 eV, the angular dependence with energy is almost completely unknown, and only one peer-reviewed article was found [20,34-36]. Regardless, our review revealed a need to update the functional form of the sputtering yield found in Ref. [9]. The sputtering yield is computed as a function of energy and angle from the product of two functions given by

$$Y\left(E,\theta\right) = Y\left(E\right)Y\left(\theta\right), \tag{5}$$

where *Y(E)* is the energy dependent yield for ions impacting the wall at normal incidence and *Y(θ)* is the angle dependent yield relative to normal incidence. The energy dependent yield is computed from

$$Y\left(E\right) = A\sqrt{E}\left(1-\sqrt{\frac{E_{th}}{E}}\right)^{2.5}, \tag{6}$$

where E is the total energy of an ion impacting the wall and the coefficients A and E_{th} are coefficients fit to experimental data. Here, E_{th} is interpreted as the threshold energy below which sputtering does not occur. The angle dependent yield is computed using the functional form suggested by Pencil, et al [37] given by

$$Y\left(\theta\right) = 1 + c_o\left(1-\cos\left(c_1\theta\right)\right)^{\kappa}, \tag{7}$$

where θ is the angle relative to the wall normal and c_o, c_1, and κ are coefficients fit to experimental data.

Given the aforementioned uncertainty in the available data, it should be noted that the sputtering yield is essentially a free parameter in any Hall thruster erosion calculation. The problem with this is that the magnitude of the yield at normal incidence, the threshold energy, and the angle dependence all strongly influence the computed erosion. In the future, we will conduct a sensitivity analysis considering how different yields affect our results, but for now we have chosen a set of curve fit coefficients from the literature for the wall material of the BPT-4000 and have found good agreement with experiment.

C. Doubly-Charged Ions

For discharge voltages around 300 V, it is common practice in the literature to neglect the effects of multiply-charged ion species on the plasma response. This approximation is usually justified based on experimental data showing that the species fraction of doubly-charged ions is about 6-11% at this voltage.

However, it has been observed that the fraction of multiply-charged ion species increases with discharge voltage [38]. Further, we discuss in a companion paper how the inclusion of doubly-charged ions, even at 300 V, is critical to our interpretation of transport mechanisms and should therefore be included [17].

Previous work at JPL using HPHall-2 ran the simulation with singly-charged ions for SPT-100 geometries [9-11]. We have since activated the doubly-charged ion species option in HPHall-2 since the BPT-4000 is presently rated for operation as high as 400 V and there is a need to model other high voltage Hall thrusters.

D. $Xe^{+} \rightarrow Xe^{2+}$ Ionization Cross-Section

In the absence of finding experimental data in the literature, Fife [15] made an "educated guess" in the original version of HPHall for the ionization cross-section of singly- to doubly-charged xenon ($Xe^{+} \rightarrow Xe^{2+}$) that underestimated the ionization rate compared with the experimental data of Bell, et al [39]. Figure 3 compares the ionization rate parameter from Fife with that of Bell, et al. For electron temperatures of 10-30 eV, Fife underestimates the ionization rate parameter by a factor of three to five. This change significantly alters the predicted ion current in the channel. The impact of these changes are discussed further in a companion paper [17]. We have updated the Xe^{+} ionization rate parameter in HPHall-2 using the algorithm suggested by Bell, et al [39].

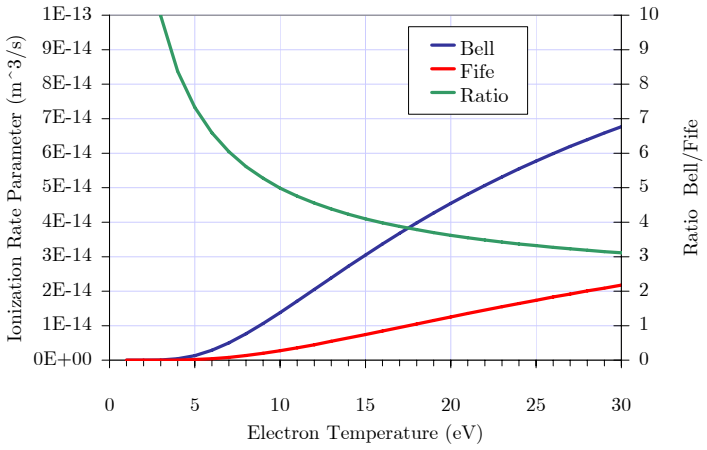

Figure 3. Xe^{+} ionization rate parameter based on measured cross-sections from Bell, et al [39] compared with the estimates made by Fife in the original version of HPHall [15].

E. Electron-Neutral Cross-Section

Since the original version of HPHall [15], an energy independent cross-section for electron-neutral scattering for xenon of 30×10^{-20} m^2 has been used. We have replaced this cross-section with a Maxwellian average of the measured energy dependent cross-sections of Nickel, et al. [40]. The expression used now in HPHall-2 is an analytical fit given by

$$Q_{e-n} = \begin{cases} 33.9581 \times 10^{-20} & T_e < 5\ eV \\ 10^{-20}\left(11.3596 + 28.0985 * e^{-0.0433494 * T_e}\right) & T_e \geq 5\ eV \end{cases}, \tag{8}$$

where T_e is the electron temperature in eV and Q_{e-n} is in m^2. Since the experimental data does not extend below 5 eV, the cross-section is set to a constant value for electron temperatures less than 5 eV.

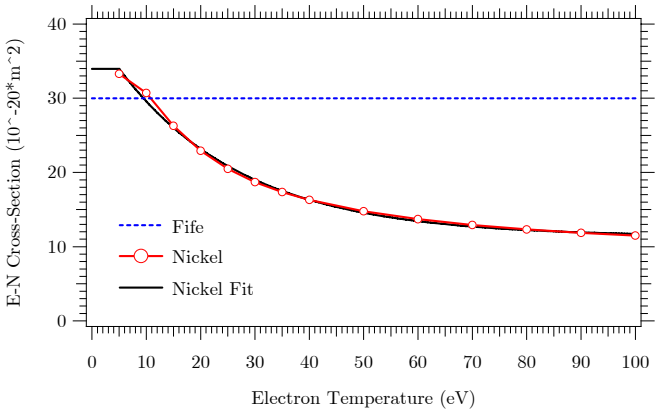

Figure 4. Maxwellian averaged cross section for electron-neutral scattering of xenon from Nickel, et al [40] compared with the analytical fit now used in HPHall-2. The constant cross-section originally used by Fife [15] is also shown.

F. Enforcement of the Bohm Condition

Parra and Ahedo first proposed in Ref. [41] that the ion velocity at the edge of the computational boundary must at least be sonic. This is enforced in HPHall-2 by requiring that the particle density at the walls is at least equal to

$$n_{eQ} = \frac{j_{riQ}}{e v_{Bohm}}, \tag{9}$$

where j_{riQ} is the radial current density of ions impacting the wall and v_{Bohm} is the Bohm velocity given by

$$v_{Bohm} = \sqrt{ZkT_e / m_i}\ . \tag{10}$$

Upon activating the doubly-charged ion model, it was observed that the ion Mach number had diverged significantly to a value of around 40. In fact, the code was over predicting the ion Mach number for solutions without doubly-charged ions (producing Mach numbers of 4-6), the problem was just not as apparent as when doubly-charged ions were activated. The problem stemmed from an incorrect implementation of the Bohm condition forcing. For a given time step, the code was computing the correct density and then immediately re-computing the ion velocity at the walls rather than letting the code converge to the correct velocity over successive time steps. We have corrected this in HPHall-2 and have also implemented a scheme originally proposed by Gamero-Castano, et al in Ref. [9] that sets the density according to

$$n_{eQ} = \beta\left(\frac{j_{riQ}}{ev_{Bohm}}\left(1+\alpha\left(\frac{v_{riQ}}{v_{Bohm}}-1\right)\right)\right), \tag{11}$$

where α and β are free parameters chosen to accelerate the convergence of the solution. We find good results with $\alpha = 1.5$ and $\beta = 0.1$, but caution that an overly aggressive choice of these parameters can lead to non-physical results at the wall boundary. As a check, we verify that the computed wall collision frequency is close to the analytical expression give by Eqn. (18) below. After making these updates, the ion Mach number is less than 2.

G. Electron Mobility Modeling

We have recently reported on efforts to modify the electron mobility model used in HPHall-2 with the aim of more accurately reproducing the spatial and temporal distributions of the plasma parameters [10,11]. In this section, we review the mobility model and the details of how it was implemented on the BPT-4000.

The cross-field electron mobility is given by

$$\mu_{e\perp} = \frac{e}{\nu_e m_e}\left(\frac{1}{1+\Omega_e^2}\right), \tag{12}$$

where ν_e is the electron collision frequency, Ω_e is the electron Hall parameter, and the rest of the symbols have their usual meaning. Wall collisions and turbulent plasma fluctuations are known to enhance the cross-field mobility in Hall thrusters. Including these effects can be accomplished by using an effective electron collision frequency given by

$$\nu_e = \nu_{eff} \equiv \nu_{en} + \nu_{ei} + \nu_w + \nu_b\ , \tag{13}$$

where ν_{en} is the electron-neutral collision frequency, ν_{ei} is the electron-ion collision frequency, ν_w is the collision frequency of the electrons with the lateral walls, and ν_b is a collision frequency defined to capture the bulk effects of turbulent plasma fluctuations.

The electron-neutral collision frequency is modeled in HPHall-2 as

$$\nu_{en} = n_n Q_{en}\sqrt{\frac{8kT_e}{\pi m_e}}\ , \tag{14}$$

where Q_{en} is the energy dependent cross-section given by Eqn. (8).

The electron-ion collision frequency is modeled in HPHall-2 as [42]

$$\nu_{ei} = 2.91\times10^{-12}\,\mathrm{n_e}\mathrm{T_e}^{-3/2}\ln\Lambda\ , \tag{15}$$

with the electron temperature in eV and the Coulomb logarithm given by

$$\ln\Lambda = \begin{cases} 23 - \log\left(T_e^{-3/2}\sqrt{10^{-6}n_e}\right) & T_e \le 10\ \text{eV} \\ 24 - \log\left(T_e^{-1}\sqrt{10^{-6}n_e}\right) & T_e > 10\ \text{eV} \end{cases}. \tag{16}$$

The wall collision frequency is modeled in HPHall-2 as

$$\nu_w = \frac{1}{\Delta \mathrm{V}}\left[\frac{\Delta A}{n_e}\Gamma_{rsW}\right]S_3 \bigcup S_4 = \frac{1}{\Delta \mathrm{V}}\left[\frac{\Delta A}{n_e}\frac{\delta_w}{1-\delta_w}\Gamma_{riQ}\right]S_3 \bigcup S_4 \,, \tag{17}$$

where ΔA and ΔV are area and volume elements between a pair of magnetic field lines sharing area elements S_3 and S_4 and the rest of the symbols have their usual meaning [16]. Note that, for a channel of width h, the above expression simplifies to

$$\nu_w \approx \frac{2\delta_w}{h\left(1-\delta_w\right)}\sqrt{\frac{kT_e}{m_i}} \,, \tag{18}$$

when the radial magnetic field is purely radial, the wall sheaths are symmetric, and the ion velocity entering the sheath is sonic.

Anomalous Bohm-like diffusion is modeled in HPHall-2 as

$$\nu_b = \frac{1}{16}\alpha\omega_{ce} \,, \tag{19}$$

where α is a parameter that can be adjusted to match experiment so that the necessary amount of cross-field diffusion results. In the case of classic Bohm diffusion, α would be equal to 1.

Experiments suggest that the parameter α varies between the plasma bounded by the discharge chamber walls and the plasma expanding downstream of the channel exhaust [43-45]. In Ref. [10,11], we reported on a mixed-mobility approach, similar to Hagelaar, et al. and Koo, et al. [46,47], which modeled turbulent fluctuations in two distinct regions separated by the exit plane of the discharge chamber. That is, α is defined according to

$$\alpha = \begin{cases} \alpha_c & z \le z_c \\ \alpha_c f_c + \alpha_p f_p & z_c < z < z_p \\ \alpha_p & z \ge z_p \end{cases} \,, \tag{20}$$

where the subscripts c and p refer to channel and plume values, respectively, z is axial position, and the fractions f are defined by

$$\begin{aligned} f_c &= 1 - f_p \\ f_p &= \frac{z - z_c}{z_p - z_c} \,. \end{aligned} \tag{21}$$

This allows the transition between the channel and plume parameters to vary smoothly over a distance z_p-z_c. For the BPT-4000 simulations presented here, a transition region of several millimeters was used while setting α_p=*1.0*. The value for α_c was chosen to match the BOL performance of the BPT-4000 operating at 300 V, 15 A. The resulting axial dependence of the collision frequency is qualitatively similar to the one shown in Ref. [11] for an SPT-100.

V. Plasma Modeling Results and Discussion

HPHall-2 was used to simulate the discharge chamber and near-field plume regions of the BPT-4000 for each of the operating conditions of the QLT. The input file for the simulations was set to best match the 4.5 kW, 300 V operating conditions. To simulate the other conditions, only the mass flow rate and channel Bohm parameter (α_c) were modified. Table 6 compares the results of HPHall-2 simulations for the QLT operating conditions. At 4.5 kW, 300 V, the agreement is excellent and at the other conditions the difference in the computed thrust varies by only 2-4%. Future modifications to the input files to better match cathode potentials, wall temperatures, and other experimental quantities will likely decrease the thrust differences.

Table 6. BPT-4000 performance from experiment and simulation for the QLT operating conditions.

	Discharge Voltage (V)	Discharge Current (A)	Thrust (mN)	Thrust Difference (%)
BPT-4000 (BOL)	300	15	291	
HPHall-2	300	15	290	-0.3%
BPT-4000 (BOL)	300	10	199	
HPHall-2	300	10	191	-4.0%
BPT-4000 (BOL)	400	11.3	253	
HPHall-2	400	11.3	249	-1.6%
BPT-4000 (BOL)	400	7.5	174	
HPHall-2	400	7.5	167	-4.0%

Table 7 lists the maximum values of several plasma properties from the simulations. The total ionization rate is dominated by the production of singly-charged ions and with the updated cross-section the ionization of singly-charged xenon is nearly an order of magnitude greater than double ionization of neutral xenon. The electron temperature is consistent with the usual scaling of $T_e \sim 0.1\ V_d$ [43-45,48,49] and the plasma density is typical of other Hall thrusters. The electron Hall parameter is consistent with values computed from measurements of other high-efficiency Hall thrusters [38].

Table 7. Maximum values of several plasma properties from HPHall-2 simulations.

Total ionization rate (m^-3 s-1)	1.6×10^{24}
$Xe^0 \rightarrow Xe^+$ ionization rate (m^-3 s-1)	1.5×10^{24}
$Xe^+ \rightarrow Xe^{2+}$ ionization rate (m^-3 s-1)	1.8×10^{23}
$Xe^0 \rightarrow Xe^{2+}$ ionization rate (m^-3 s-1)	2.9×10^{22}
Electron temperature (eV)	32
Plasma density (m^-3)	3.6×10^{18}
Electron Hall parameter	190

Aside from these global parameters, several other plasma properties were extracted from the model for analysis of the various utilization efficiencies. We will use a performance model similar to the one proposed by Hofer and Gallimore in Ref. [38] and recently modified by Jameson, et al [50] to explicitly include the effects of beam divergence in analysis of a 6 kW Hall thruster. In this description of Hall thruster performance, the anode efficiency is given by the product of several utilization efficiencies given by

$$\eta_a = \gamma^2 \eta_v \eta_b \eta_m \,, \tag{22}$$

where the partial efficiencies are the total thrust correction factor expressed as the product of the multiply-charged ion correction factor and plume divergence correction factor given by

$$\gamma = \alpha_t F_t = \sum \frac{\Omega_i}{\sqrt{Z_i}} \cos\theta \,, \tag{23}$$

the voltage utilization efficiency

$$\eta_v = \frac{V_a}{V_d} = 1 - \frac{V_l}{V_d} \,, \tag{24}$$

the current utilization efficiency

$$\eta_b = \frac{I_b}{I_d} \,, \tag{25}$$

and the mass utilization efficiency

$$\eta_m = \frac{\dot{m}_b}{\dot{m}_a} = \eta_b \left(\frac{m_{xe} I_d}{\dot{m}_a e} \right) \sum \frac{\Omega_i}{Z_i} = \eta_b (\xi) \alpha_m \,. \tag{26}$$

In the above, the plume divergence angle is defined according to [51]

$$\cos\theta = \frac{\int_0^{2\pi} \int_{R_i}^{R_o} j_z r dr d\theta}{\int_0^{2\pi} \int_{R_i}^{R_o} \left| \vec{j} \right| r dr d\theta} = \frac{\int_{R_i}^{R_o} j_z r dr}{\int_{R_i}^{R_o} \left| \vec{j} \right| r dr} \,, \tag{27}$$

where the limits of integration, R_i and R_o, are chosen based on the limits of the computational domain, j_z is the axial component of the ion current density, and $\vec{j}$ is the ion current density vector. The integration plane is chosen at an axial location near the edge of the computational boundary.

Table 8 through Table 11 present several thruster performance properties derived from the simulations. Table 8 lists various properties of the currents in the thruster. The 24 kHz breathing-mode frequency is typical for 300 V discharges and the magnitude of the oscillations is also consistent with measured values from the BPT-4000 and other thrusters [25,38,52]. Table 9 lists the species fractions and related correction factors. The doubly-charged xenon current fraction of 25% is consistent with the literature [38,53-56].

Table 10 lists the total plume divergence half-angle and the divergence angles for singly- and doubly-charged xenon. The divergence angle defined here should not be confused with divergence angles derived from far-field plume measurements that are used to study spacecraft interactions [52]. The divergence angle of doubly-charged xenon is about three degrees larger than the singly-charged xenon since the doubles are created further downstream. A larger divergence angle for the multiply-charged species in Hall thruster plumes is well documented [53-56].

Finally, using the data in the previous tables, Table 11 presents the various utilization efficiencies computed from the HPHall-2 simulation. The current and mass utilizations are slightly higher than measured by Hofer in Ref. [38] on a different high-efficiency Hall thruster, but are not unreasonable. The total thrust correction, voltage utilization, and mean acceleration voltage of 289 V are consistent with other experimental data, including data taken with the BPT-4000 [38,53-56].

The plasma properties and integral performance of the BPT-4000 predicted by HPHall-2 are in general agreement with measured data from the BPT-4000 or other thrusters in its power class. Taken together, these results indicate that HPHall-2 is providing a sufficiently accurate prediction of the BPT-4000 plasma properties to serve as a reliable input for erosion calculations.

Table 8. Ion and electron current properties from HPHall-2 simulations.

Discharge Current (A) =	15.02
Beam Current (A) =	12.47
Xe^{+} Current (A) =	9.41
Xe^{2+} Current (A) =	3.06
Electron Current (A) =	2.54
Breathing Mode Frequency (kHz) =	24
Discharge Current Standard Deviation (A) =	1.9
Peak-to-Peak Discharge Current Oscillations (A) =	10.5
Exchange Ratio =	1.32

Table 9. Species current fractions and correction factors from HPHall-2 simulations.

Xe^{+} Current Fraction =	0.75
Xe^{2+} Current Fraction =	0.25
α_t =	0.93
α_m =	0.88

Table 10. Divergence half-angles and thrust correction factor from HPHall-2 simulations.

Divergence half-angle (deg) =	17.5
Xe^{+} divergence half-angle (deg) =	16.6
Xe^{2+} divergence half-angle (deg) =	20.3
Thrust correction factor =	0.954

Table 11. Utilization efficiencies from HPHall-2 simulations.

γ^2 =	0.78
Current Utilization =	0.83
Mass Utilization =	0.96
Voltage Utilization =	0.96
Effective Acceleration Voltage (V) =	289

VI. Erosion Modeling Results and Discussion

Using the results from the plasma model as inputs, the time-dependent erosion of the BPT-4000 discharge chamber walls was simulated for the initial 4.5 kW, 300 V operating condition of the QLT. The erosion sub-model used was an evolved version of the one developed by Gamero-Castano, et al [9]. An erosion calculation proceeds according to the flow diagram shown in Figure 5. After constructing the initial grid and magnetic field, HPHall-2 is used to compute the ion particle flux to the wall boundaries. This ion flux is then imported into the erosion sub-model and used to compute the wall erosion rates, which are used to move the wall boundaries in the radial and axial directions. The new geometry is then used as the input for a new computational grid and magnetic field. The entire process is then repeated by again running the plasma simulation. In our simulations, we are careful to allow the plasma simulation enough iterations to reach a new steady-state after moving the grid. The time step for advancing the wall also must be carefully chosen to avoid introducing instabilities in the wall erosion, especially at BOL when the erosion rates are greatest. Throughout this process, the Bohm parameters are kept constant and only the mass flow rate is changed to reflect the actual conditions of the test. This is important since the mass flow rate at the 4.5 kW, 300 V condition changed by ~14% over the course of the QLT (not shown, see Ref. [6,7]).

Figure 6 and Figure 7 compare the BPT-4000 wall erosion from experiment and simulation for the inner and outer walls, respectively. Simulation data is shown at 68, 400, and 993 h only in order to compare with the available experimental data although smaller time steps were taken in between these times. On the inner wall, excellent agreement is found between the experiment and simulation. On the outer wall, the simulation was within the uncertainty of the data until 400 h, but overall the erosion progressed at a slower rate than the data, only progressing about 62% of the radial distance needed to match experiment after 993 h. However, the erosion rate over the last few hundred hours was

accelerating along the outer wall. This may indicate that the outer wall erosion will "catch up" with the experimental data within the next several hundred hours. Simulations are continuing at this time with the aim of extending the runs to the end of the QLT-E.

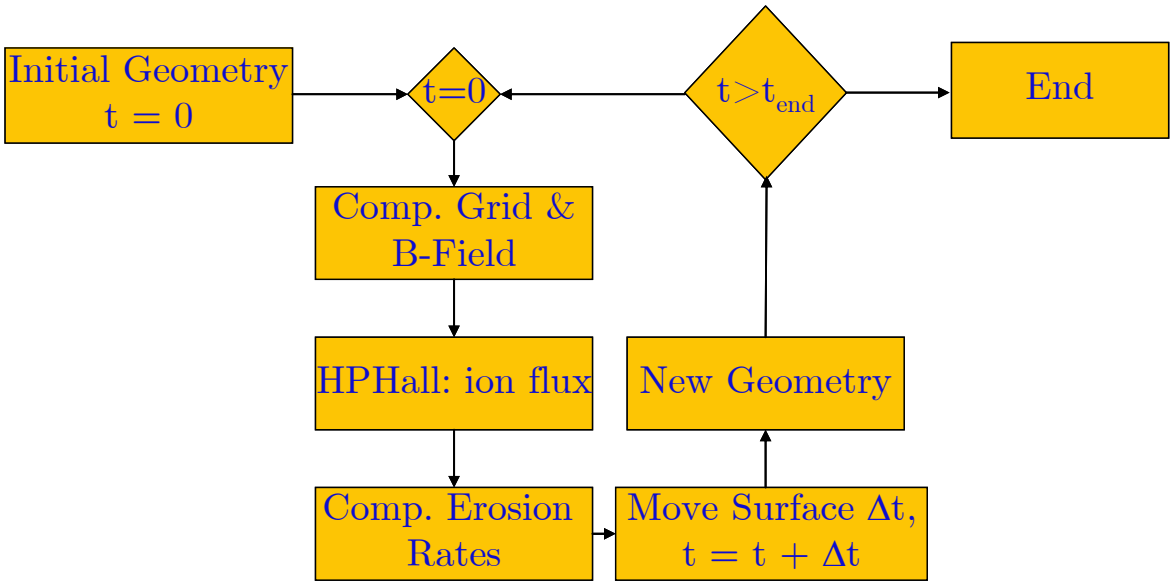

Figure 5. Flow diagram for erosion calculations [9].

Table 12 through Table 14 list properties of the wall erosion process after 68, 400, and 993 hours of operation, respectively. Properties are shown for a node near the upstream boundary of the erosion zone and for the node at the exit plane of the thruster. As one might expect, there are significant differences in the erosion properties depending on the axial location.

At the upstream boundary, the total ion energy is between 36-48 eV, of which, between 54-78% is due to the sheath potential. This highlights the need to not only have accurate knowledge of the low-energy behavior of the sputtering yield, but also physically representative sheath models. When these elements are absent, the upstream boundary of the erosion zone is often miscalculated.

At the exit plane, the total ion energy is between 133-184 eV, of which, approximately 77-82% is due to the drift energy of the ions. This indicates that much of the wall erosion process near the exit plane is dominated by the drift energy of the ions. However, it is at most 82% of the problem, so any model that neglects the sheath potential and still manages to match experimental data is likely overestimating some other quantity like the sputtering yield.

In terms of the erosion rate, it is interesting to note that the inner wall rate at the exit plane increases between 68 and 400 h while the outer wall rate at the exit plane is still increasing at 993 h. An examination of the experimental data indicates that the wall erosion rate observed during the QLT is also a non-monotonic function of time. A more detailed examination of this behavior is currently being conducted.

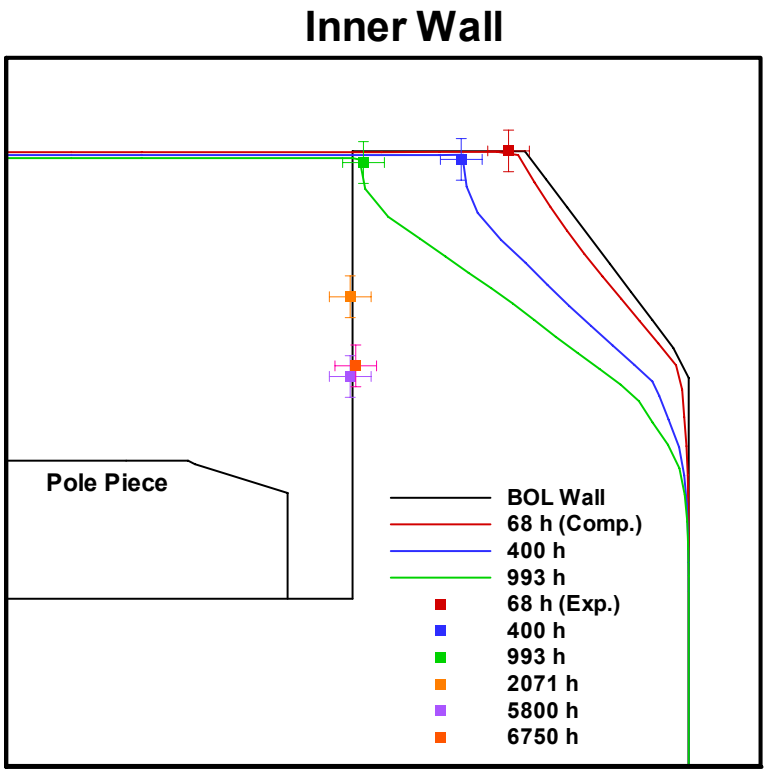

Figure 6. Comparison of BPT-4000 inner wall erosion from experiment and simulation.

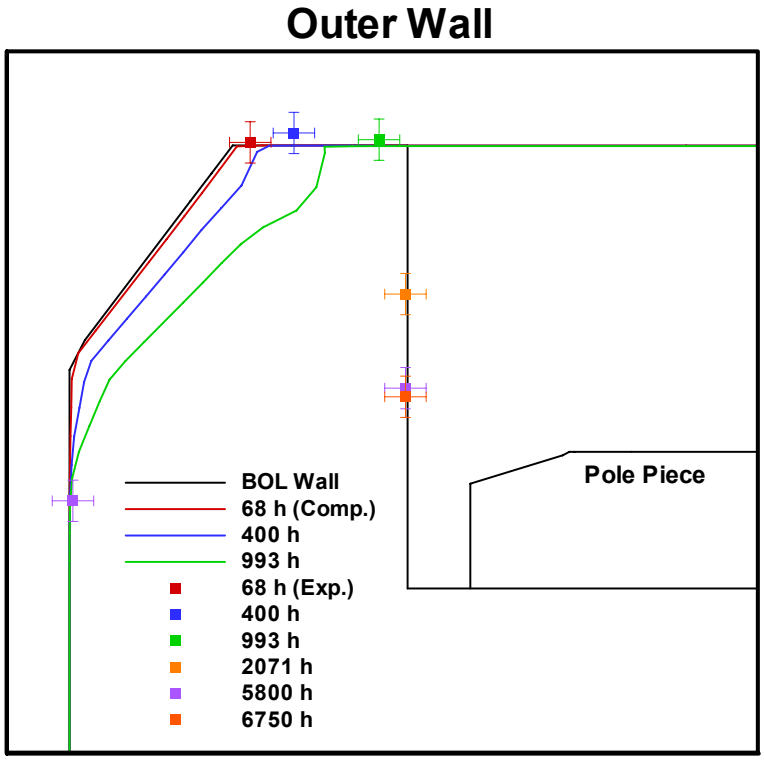

Figure 7. Comparison of BPT-4000 outer wall erosion from experiment and simulation.

Table 12. Properties of the wall erosion after 68 h of simulated operation.

	Upstream Boundary		Exit Plane	
	Inner Wall	Outer Wall	Inner Wall	Outer Wall
Drift Energy (eV)	22	18	102	108
Sheath Energy (eV)	26	24	31	28
Total Energy (eV)	48	42	133	136
Impact Angle (Deg)	23	22	29	35
Erosion Rate* (-)	0.32	0.12	1.00	0.41
*Relative to the inner wall exit plane at t=68 h.				

Table 13. Properties of the wall erosion after 400 h of simulated operation.

	Upstream Boundary		Exit Plane	
	Inner Wall	Outer Wall	Inner Wall	Outer Wall
Drift Energy (eV)	13	12	126	133
Sheath Energy (eV)	24	24	30	30
Total Energy (eV)	37	36	156	163
Impact Angle (Deg)	23	20	24	34
Erosion Rate* (-)	0.15	0.09	1.29	0.74
*Relative to the inner wall exit plane at t=68 h.				

Table 14. Properties of the wall erosion after 993 h of simulated operation.

	Upstream Boundary		Exit Plane	
	Inner Wall	Outer Wall	Inner Wall	Outer Wall
Drift Energy (eV)	8	10	112	147
Sheath Energy (eV)	29	26	28	37
Total Energy (eV)	37	36	140	184
Impact Angle (Deg)	14	16	16	27
Erosion Rate* (-)	0.03	0.21	1.00	0.88
*Relative to the inner wall exit plane at t=68 h.				

Although doubly-charged ions play a key role in the performance of Hall thrusters [17,38], in our simulations of the BPT-4000 they play almost no role in the erosion process. At BOL, the ratio of the particle flux of singly-to-doubly charged ions is about 36-40 at the upstream boundary of the erosion zone and about 12-17 at the exit plane. The reason for the decline in this ratio with axial distance is that the

doubles are born further downstream than the singles, so they gradually participate more in the erosion as we progress downstream. Although doubles do not play a direct role in the erosion, they do significantly affect the plasma response that is the input to the erosion calculation. Further, we note that the role of multiply-charged ions in the erosion process is expected to increase with discharge voltage as the fraction of multiply-charged ions increases and the ionization layer grows in axial extent [57]. A companion paper further discusses the role of ion current in Hall thrusters [17].

Conclusion

Driven by the simple fact that qualification life testing almost never exactly matches the mission profile on the first use of a technology (let alone the n^{th} use), a set of plasma and erosion modeling tools for Hall thrusters are being developed. The complexity of erosion processes and failure modes in these systems requires the availability of physics-based models that can accurately simulate the behavior observed during ground testing as well as serve as a predictive tool for actual mission profiles. The recent interest in Hall thrusters for NASA science missions has revealed a need to develop and maintain these tools internal to the agency.

Our approach has intentionally avoided semi-empirical or low-order fluid models that fail to capture enough of the relevant physics to be solely relied on as a predictive tool for missions costing hundreds of millions of dollars. In order for our models to be relied on as accurate representations of thruster physics, it is necessary, at a minimum, that they reproduce accurately the time-averaged distribution and magnitudes of plasma properties in the channel as well as the performance and erosion observed over the throttling range.

Updated versions of a physics-based set of plasma and erosion modeling tools have been applied to the BPT-4000 Hall thruster and shown to be accurate representations of the relevant thruster physics. Our results show that both models can reproduce the measured thruster properties and performance. Several important changes to the collision cross-sections, secondary electron emission yields, sputtering yields, Bohm condition enforcement, and the activation of the doubly-charged ion model have improved the fidelity of our simulations. Application to the BPT-4000 has shown that the updated code can accurately reproduce many of the micro- and macroscopic properties that determine the plasma response and thruster performance over a wide range of power and voltages. An erosion simulation carried through almost 1000 hours of thruster operation has shown general agreement overall with experiment. Analysis of wall erosion properties reveals that the process is both spatially and temporally dependent, which verifies the importance of developing modeling tools that are physics-based and capable of predicting the complexity of Hall thruster erosion physics.

Acknowledgments

The research described in this paper was carried out at the Jet Propulsion Laboratory, California Institute of Technology, under a contract with the National Aeronautics and Space Administration. This

work was supported by the NASA In-Space Propulsion program and was managed by Eric Pencil (NASA GRC), technology area manager for Solar Electric Propulsion.

References

[1] Hofer, R. R., Randolph, T. M., Oh, D. Y., Snyder, J. S., and de Grys, K. H., "Evaluation of a 4.5 kW Commercial Hall Thruster System for NASA Science Missions," AIAA Paper 2006-4469, July 2006.

[2] Oh, D. Y. and Goebel, D. M., "Performance Evaluation of an Expanded Throttle Range XIPS Ion Thruster System for NASA Science Missions," AIAA Paper 2006-4466, July 2006.

[3] Oh, D. Y., "Evaluation of Solar Electric Propulsion Technologies for Discovery-Class Missions," Journal of Spacecraft and Rockets **44**, 2, 399-411 (2007).

[4] Randolph, T. M., "Qualification of Commercial Electric Propulsion Systems for Deep Space Missions," Presented at the 30th International Propulsion Conference, IEPC Paper 2007-271, Florence, Italy, Sept. 17-20, 2007.

[5] Sengupta, A., Brophy, J. R., Anderson, J. R., Garner, C., de Groh, K. et al., "An Overview of the Results from the 30,000 Hr Life Test of Deep Space 1 Flight Spare Ion Engine," AIAA Paper 2004-3608, July 2004.

[6] de Grys, K. H., Welander, B., Dimicco, J., Wenzel, S., Kay, B. et al., "4.5 kW Hall Thruster System Qualification Status," AIAA Paper 2005-3682, July 2005.

[7] Welander, B. A. and de Grys, K. H., "Completion of the BPT-4000 Hall Thruster Qualification," Presented at the 53rd JANNAF Propulsion Meeting, Monterey, CA, Dec. 5-8, 2005.

[8] Welander, B., Carpenter, C., de Grys, K. H., Hofer, R. R., Randolph, T. M. et al., "Life and Operating Range Extension of the BPT-4000 Qualification Model Hall Thruster," AIAA Paper 2006-5263, July 2006.

[9] Gamero-Castano, M. and Katz, I., "Estimation of Hall Thruster Erosion Using HPHall," Presented at the 29th International Electric Propulsion Conference, IEPC Paper 2005-303, Princeton, NJ, Oct. 31-Nov. 4, 2005.

[10] Hofer, R. R., Katz, I., Mikellides, I. G., and Gamero-Castano, M., "Heavy Particle Velocity and Electron Mobility Modeling in Hybrid-PIC Hall Thruster Simulations," AIAA Paper 2006-4658, July 2006.

[11] Hofer, R. R., Mikellides, I. G., Katz, I., and Goebel, D. M., "Wall Sheath and Electron Mobility Modeling in Hybrid-PIC Hall Thruster Simulations," AIAA Paper 2007-5267, July 2007.

[12] Katz, I., Mikellides, I. G., Wirz, R., Anderson, J. R., and Goebel, D. M., "Ion Thruster Life Models," AIAA Paper 2005-4256, July 2005.

[13] Gnizdor, R., Kozubsky, K., Koryakin, A., Maslenikov, N., Pridannikov, S. et al., "SPT-100 Life Test with Single Cathode up to Total Impulse Two Million Nsec," AIAA Paper 1998-3790, July 1998.

[14] Cornu, N., Marchandise, F., Darnon, F., and Estublier, D., "The PPS-1350-G Qualification Demonstration: 10500 Hrs on the Ground and 5000 Hrs in Flight," AIAA Paper 2007-5197, July 2007.

[15] Fife, J. M., "Hybrid-PIC Modeling and Electrostatic Probe Survey of Hall Thrusters," Ph.D. Thesis, Aeronautics and Astronautics, Massachusetts Institute of Technology, 1998.

[16] Parra, F. I., Ahedo, E., Fife, J. M., and Martinez-Sanchez, M., "A Two-Dimensional Hybrid Model of the Hall Thruster Discharge," Journal of Applied Physics **100**, 023304 (2006).

[17] Katz, I., Hofer, R. R., and Goebel, D. M., "Ion Current in Hall Thrusters," Presented at the 30th International Electric Propulsion Conference, IEPC Paper 2007-365, Florence, Italy, Sept. 17-20, 2007.

[18] Yim, J. T., Keidar, M., and Boyd, I. D., "A Hydrodynamic-Based Erosion Model for Hall Thrusters," Presented at the 29th International Electric Propulsion Conference, IEPC Paper 2005-013, Princeton, NJ, Oct. 31 - Nov. 4, 2005.

[19] Manzella, D., Yim, J. T., and Boyd, I. D., "Predicting Hall Thruster Operational Lifetime," AIAA Paper 2004-3953, July 2004.

[20] Abgaryan, V., Kaufman, H. R., Kim, V., Ovsyanko, D., Shkarban, I. et al., "Calculation Analysis of the Erosion of the Discharge Chamber Walls and Their Contamination During Prolonged SPT Operation," AIAA Paper 94-2859, July 1994.

[21] Lovtsov, A. A., Shagayda, A. A., and Gorshkov, O. A., "Semi-Empirical Method of Hall Thrusters Lifetime Prediction," AIAA Paper 2006-4661, July 2006.

[22] Sommier, E., Allis, M. K., Gascon, N., and Cappelli, M. A., "Wall Erosion in 2D Hall Thruster Simulations," AIAA Paper 2006-4656, July 2006.

[23] Cheng, S. Y., "Modeling of Hall Thruster Lifetime and Erosion Mechanisms," Ph.D. Thesis, Aeronautics and Astronautics, Massachusetts Institute of Technology, 2007.

[24] Welander, B., "Qualification Test Report - General Release - Hall Thruster Propulsion System, BPT-4000 Hall Current Thruster," Aerojet, 2006-R-2791, Dec. 2006.

[25] de Grys, K., Rayburn, C., Wilson, F., Fisher, J., Werthman, L. et al., "Multi-Mode 4.5 kW BPT-4000 Hall Thruster Qualification Status," AIAA Paper 2003-4552, July 2003.

[26] Gascon, N., Dudeck, M., and Barral, S., "Wall Material Effects in Stationary Plasma Thrusters I: Parametric Studies of an SPT-100," Physics of Plasmas **10**, 10, 4123-4136 (2003).

[27] Barral, S., Makowski, K., Peradzynski, Z., Gascon, N., and Dudeck, M., "Wall Material Effects in Stationary Plasma Thrusters II: Near-Wall and in-Wall Conductivity," Physics of Plasmas **10**, 10, 4137-4152 (2003).

[28] Kim, V., Kozlov, V., Skrylnikov, A., Veselovzorov, A., Hilleret, N. et al., "Investigation of Operation and Characteristics of Small SPT with Discharge Chamber Walls Made of Different Ceramics," AIAA Paper 2003-5002, July 2003.

[29] Dunaevsky, A., Raitses, Y., and Fisch, N. J., "Secondary Electron Emission from Dielectric Materials of a Hall Thruster with Segmented Electrodes," Physics of Plasmas **10**, 6, 2574-2577 (2003).

[30] Bugeat, J. P. and Koppel, C., "Development of a Second Generation of SPT," Presented at the 24th International Electric Propulsion Conference, IEPC Paper 1995-35, Moscow, Russia, Sept. 19-23, 1995.

[31] Viel-Inguimbert, V., "Secondary Electron Emission of Ceramics Used in the Channel of SPT," Presented at the 28th International Electric Propulsion Conference, IEPC Paper 2003-258, Toulouse, France, Mar. 17-23, 2003.

[32] Taccogna, F., Longo, S., and Capitelli, M., "Plasma Sheaths in Hall Discharge," Physics of Plasmas **12**, 093506 (2005).

[33] Dawson, P. H., "Secondary Electron Emission Yields of Some Ceramics," Journal of Applied Physics **37**, 3644-3645 (1966).

[34] Garnier, Y., Viel, V., Roussel, J. F., and Bernard, J., "Low-Energy Xenon Ion Sputtering of Ceramics Investigated for Stationary Plasma Thrusters," Journal of Vacuum Science and Technology A **17**, 6, 3246-3254 (1999).

[35] Yalin, A. P., Rubin, B., Domingue, S. R., Glueckert, Z., and Williams, J. D., "Differential Sputter Yields of Boron Nitride, Quartz, and Kapton Due to Low Energy Xe+ Bombardment," AIAA Paper 2007-5314, July 2007.

[36] Kim, V., Kozlov, V., Semenov, A., and Shkarban, I., "Investigation of the Boron Nitride Based Ceramics Sputtering Yield under Its Bombardment by Xe and Kr Ions," Presented at the 27th International Electric Propulsion Conference, IEPC Paper 2001-073, Pasadena, CA, Oct. 15-19, 2001.

[37] Pencil, E. J., Randolph, T., and Manzella, D. H., "End-of-Life Stationary Plasma Thruster Far-Field Plume Characterization," AIAA Paper 1996-2709, July 1996.

[38] Hofer, R. R. and Gallimore, A. D., "High-Specific Impulse Hall Thrusters, Part 2: Efficiency Analysis," Journal of Propulsion and Power **22**, 4, 732-740 (2006).

[39] Bell, E. W., Djuric, N., and Dunn, G. H., "Electron-Impact Ionization of In+ and Xe+," Physical Review A **48**, 6, 4286-4291 (1993).

[40] Nickel, J. C., Imre, K., Register, D. F., and Trajmar, S., "Total Electron Scattering Cross Sections: I. He, Ne, Ar, Xe," Journal of Physics B: Atomic, Molecular and Optical Physics **18**, 125-133 (1985).

[41] Parra, F. I. and Ahedo, E., "Fulfillment of the Bohm Condition on the HPHall Fluid-PIC Code," AIAA Paper 2004-3955, July 2004.

[42] Huba, J. D., *NRL Plasma Formulary.* (Naval Research Laboratory, Washington, DC, 2007).

[43] Haas, J. M., "Low-Perturbation Interrogation of the Internal and near-Field Plasma Structure of a Hall Thruster Using a High-Speed Probe Positioning System," Ph.D. Dissertation, Aerospace Engineering, University of Michigan, 2001.

[44] Linnell, J. A., "An Evaluation of Krypton Propellant in Hall Thrusters," Ph.D. Dissertation, Aerospace Engineering, University of Michigan, 2007.

[45] Meezan, N. B., Hargus, W. A., and Cappelli, M. A., "Anomalous Electron Mobility in a Coaxial Hall Discharge Plasma," Physical Review E **63**, 026410, 1-7 (2001).

[46] Hagelaar, G. J. M., Bareilles, J., Garrigues, L., and Bouef, J. P., "Role of Anomalous Electron Transport in a Stationary Plasma Thruster Simulation," Journal of Applied Physics **93**, 1, 67-75 (2003).

[47] Koo, J. W. and Boyd, I. D., "Modeling of Anomalous Electron Mobility in Hall Thrusters," Physics of Plasmas **13**, 033501 (2006).

[48] Raitses, Y., Staack, D., Keidar, M., and Fisch, N. J., "Electron-Wall Interaction in Hall Thrusters," Physics of Plasmas **12**, 057104 (2005).

[49] Raitses, Y., Staack, D., Smirnov, A., and Fisch, N. J., "Space Charge Saturated Sheath Regime and Electron Temperature Saturation in Hall Thrusters," Physics of Plasmas **12**, 073507 (2005).

[50] Jameson, K. K., Goebel, D. M., Hofer, R. R., and Watkins, R. M., "Cathode Coupling in Hall Thrusters," Presented at the 30th International Electric Propulsion Conference, IEPC Paper 2007-278, Florence, Italy, Sept. 17-20, 2007.

[51] Goebel, D. M. and Katz, I., *Fundamentals of Electric Propulsion: Ion and Hall Thrusters*. (John Wiley & Sons, New York, 2007).

[52] Hofer, R. R. and Gallimore, A. D., "High-Specific Impulse Hall Thrusters, Part 1: Influence of Current Density and Magnetic Field," Journal of Propulsion and Power **22**, 4, 721-731 (2006).

[53] Gulczinksi, F. S. and Gallimore, A. D., "Near-Field Ion Energy and Species Measurements of a 5-kW Hall Thruster," Journal of Propulsion and Power **17**, 2, 418-427 (2001).

[54] Kim, S.-W. and Gallimore, A. D., "Plume Study of a 1.35-kW SPT-100 Using an ExB Probe," Journal of Spacecraft and Rockets **39**, 6, 904-909 (2002).

[55] King, L. B. and Gallimore, A. D., "Mass Spectral Measurements in the Plume of an SPT-100 Hall Thruster," Journal of Propulsion and Power **16**, 6, 1086-1092 (2000).

[56] Pollard, J. E., Diamant, K. D., Khayms, V., Werthman, L., King, D. Q. et al., "Ion Flux, Energy, and Charge-State Measurements for the BPT-4000 Hall Thruster," AIAA Paper 2001-3351, July 2001.

[57] Hofer, R. R., "Development and Characterization of High-Efficiency, High-Specific Impulse Xenon Hall Thrusters," Ph.D. Dissertation, Aerospace Engineering, University of Michigan, 2004. (Also NASA/CR-2004-213099)